Title
Variability of white matter anatomy in the subcallosal cingulate area

Journal
Human Brain Mapping, 42(7)

ISSN
1065-9471

Authors
Tsolaki, Evangelia
Sheth, Sameer A
Pouratian, Nader

Publication Date
2021-05-01

DOI
10.1002/hbm.25341

Peer reviewed

Received: 16 July 2020 | Revised: 16 December 2020 | Accepted: 28 December 2020

DOI: 10.1002/hbm.25341

RESEARCH ARTICLE

WILEY

Variability of white matter anatomy in the subcallosal cingulate area

Evangelia Tsolaki[1] | Sameer A. Sheth[2] | Nader Pouratian[1]

[1]Department of Neurosurgery, University of California Los Angeles, Los Angeles, California

[2]Department of Neurosurgery, Baylor College of Medicine, Houston, Texas

Correspondence
Evangelia Tsolaki, MSc, PhD, Department of Neurosurgery, University of California, Los Angeles, 300 Stein Plaza, Suite 562, Los Angeles, CA 90095.
Email: etsolaki@mednet.ucla.edu

Funding information
National Institute of Neurological Disorders and Stroke, Grant/Award Number: UH3NS103549

Abstract

The subcallosal cingulate (SCC) area is a putative hub in the brain network underlying depression. Deep brain stimulation (DBS) targeting a particular subregion of SCC, identified as the intersection of forceps minor (FM), uncinate fasciculus (UCF), cingulum and fronto-striatal fiber bundles, may be critical to a therapeutic response in patients with severe, treatment-resistant forms of major depressive disorder (MDD). The pattern and variability of the white matter anatomy and organization within SCC has not been extensively characterized across individuals. The goal of this study is to investigate the variability of white matter bundles within the SCC that structurally connect this region with critical nodes in the depression network. Structural and diffusion data from 100 healthy subjects from the Human Connectome Project database were analyzed. Anatomically defined SCC regions were used as seeds to perform probabilistic tractography and to estimate the connectivity from the SCC to subject-specific target areas believed to be involved in the pathology of MDD including ventral striatum (VS), UCF, anterior cingulate cortex (ACC), and medial prefrontal cortex (mPFC). Four distinct areas of connectivity were identified within SCC across subjects: (a) postero-lateral SCC connectivity to medial temporal regions via UCF, (b) postero-medial connectivity to VS, (c) superior-medial connectivity to ACC via cingulum bundle, and (d) antero-lateral connectivity to mPFC regions via forceps minor. Assuming white matter connectivity is critical to therapeutic response, the improved anatomic understanding of SCC as well as an appreciation of the intersubject variability are critical to developing optimized therapeutic targeting for SCC DBS.

KEYWORDS
anatomy, depression, probabilistic Tractography, subcallosal cingulate

1 | INTRODUCTION

The subcallosal cingulate (SCC) area has been strongly implicated in the pathophysiology of depression (Mayberg, 2009) given its connectivity with brain regions involved in major depressive disorder (MDD) and its key role in the processing and regulation of emotions (Drevets, Price, & Furey, 2008). Functional alterations of the SCC have been found to relate to antidepressant response to treatment (Argyelan et al., 2016; Drevets, Savitz, & Trimble, 2008). Also, MDD patients demonstrate increased SCC cerebral blood flow relative to controls (Mayberg et al., 1999; Seminowicz et al., 2004; Siegle, Carter, & Thase, 2006) while various somatic and behavioral treatment

modalities appear to decrease blood flow or glucose metabolism within the SCC (Dougherty et al., 2003; Goldapple, Segal, Garson, & Lau, 2004; Kennedy et al., 2007; Mayberg et al., 1999, 2000; Mottaghy et al., 2002; Nobler et al., 2000, 2001; Pardo et al., 2008; Wu et al., 1999).

The SCC is the most studied (Choi, Riva-Posse, Gross, & Mayberg, 2015; Holtzheimer et al., 2012; Lozano et al., 2008, 2011; Mayberg et al., 2005; Neimat et al., 2008; Puigdemont et al., 2012; Riva-Posse et al., 2014) deep brain stimulation (DBS) target area for treatment resistant depression (TRD). Despite growing interest as a therapeutic target and appreciation of widespread connectivity to the limbic system, thalamus, hypothalamus, and brainstem nuclei (Gutman, Holtzheimer, Behrens, Johansen-Berg, & Mayberg, 2009; Hamani et al., 2011) the internal anatomic organization of this region is still incompletely defined. In particular, very limited work has been done to investigate the consistency and variability of white matter tracts within this region (Johansen-Berg et al., 2007). Connectivity-based parcellation of SCC has not been investigated or described across a large cohort of subjects, particularly with a focus on variability across individuals.

Understanding the underlying neuroanatomical organization is likely of clinical importance as well. A number of studies have investigated the potential role of specific axonal pathways in mediating the anti-depressant effects of DBS. Using a SCC DBS activation model, the engagement of cortical (ventromedial prefrontal cortex, vmPFC), sub-cortical (ventral striatum [VS]), and cingulate pathways (cingulum bundle) has been suggested to be necessary to achieve improved clinical outcomes (Lujan et al., 2013). Comparisons between SCC DBS responders and nonresponders likewise suggest that when a combination of subject-specific white matter fibers are within the volume of activated tissue (forceps minor (FM), uncinate fasciculus (UCF), cingulum bundle (CM) and fronto-striatal fibers), improved clinical outcome may be expected (Riva-Posse et al., 2014; Tsolaki, Espinoza, & Pouratian, 2017). A subsequent finer grained analysis suggests that the direct activation of right CB, left CB, and FM pathways could be the most likely therapeutic pathways when targeting and stimulating SCC (Howell et al., 2019). In another study, the "best" overall response to SCC DBS was associated with structural connectivity to bilateral ventromedial frontal cortex (via UCF and FM) and cingulate cortex (via cingulum bundle) (Choi et al., 2015). As proof of importance of using subject-specific mapping, a recent pilot SCC DBS study explored the value of individualized, patient-specific, deterministic tractography targeting of SCC (Riva-Posse et al., 2018). While the relative importance of individual tracts remains to be defined, taken together these studies highlight the importance of better defining the internal white matter anatomy of the SCC and its interindividual variability more systematically, in order to define both the need for subject-specific mapping and to develop improved methods for selecting therapeutic targets within SCC.

The connectivity of SCC to these distant regions is relevant as these other regions have likewise been implicated in depression. FM contains axonal projections to the lateral and medial prefrontal cortex (mPFC) through the anterior corpus callosum, forming part of the fronto-limbic circuitry that may assist in regulating depressive symptoms (Johnstone, van Reekum, Urry, Kalin, & Davidson, 2007; Phillips, 2003). Cingulum bundle represents a major association fiber tract of the limbic-cortical networks involved in depression (Mayberg, 2003). It forms a distinctive white matter tract that appears to almost encircle the corpus callosum and enter the temporal lobe. It consists of three different subdivisions: parahippocampal, retrosplenial, and subgenual that occupy different medial–lateral locations (Jones, Christiansen, Chapman, & Aggleton, 2013). The VS has a prominent role in the reward processing pathway and maintains connectivity with other emotion generators and regions associated with the anticipation and receipt of monetary or social rewards (Izuma, Saito, & Sadato, 2008). This network is related to abnormalities in hedonic tone and motivation (Nestler et al., 2002), which are key features of depression. UCF is the largest white matter association tract connecting the prefrontal cortex and the mesial temporal lobe (Olson, Der, Alm, & Vyas, 2015; Simmonds, Hallquist, Asato, & Luna, 2014; Von Der Heide, Skipper, Klobusicky, & Olson, 2013) and it is characterized by reduced white matter integrity in the subgenual stem in depression (Bhatia, Henderson, Hsu, & Yim, 2018).

Given the role of SCC in a dense neural network of high relevance to the clinical and behavioral manifestations of MDD, understanding the neuroanatomy of white matter pathways within SCC is important. This anatomic understanding of variability will provide a key framework for informing our understanding of this critical brain region as well as potentially provide a critical reference for the design of future clinical trials. Importantly, we remain agnostic about the clinical relevance of each pathway and believe that our functional understanding will evolve with further clinical trials and experience. The goal of this study is to characterize the underlying pattern and interindividual variability of white matter pathways within SCC with an eye toward the relevance of this anatomy for individualized DBS targeting for simultaneous engagement of multiple white matter pathways.

2 | METHODS

2.1 | Imaging data

An informed consent form was obtained from all subjects. Each subject underwent MR imaging using a multi-slice spin-echo sequence with multi-band where each gradient table included approximately 90 diffusion-weighted directions plus 6 b0 acquisitions interspersed within each run (field of view (FOV) = $210 \times 180 \times 138$ mm^3, b value = 0, 1,000, 2,000, 3,000 s/mm^2, voxel size = $1.25 \times 1.25 \times 1.25$ mm^3, repetition time/echo time = 5,520/289.5 ms, flip angle (FA) = 78°, refocusing flip angle (rFA) = 160°, Bandwidth (BW) = 1,488 Hz per pixel, multiband factor = 3, echo spacing (ES) = 0.78 ms, and gradient strength = 100 mT/m) and a high resolution, motion corrected multi-echo MPRAGE T1-weighted sequence (TEs/TR = 2.14/2400 ms, TI = 1,000 ms, FA = 8°, FOV = $180 \times 224 \times 224$ mm^3, voxel size = $0.7 \times 0.7 \times 0.7$ mm^3). The preprocessed data with respect

to image distortion correction and registration to common structural space were used from the HCP database.

2.2 | Definition of seed and target areas

SCC seed: Anatomical SCC seed regions were initially defined as $5 \times 5 \times 5$ voxel ROIs centered at $x = \pm 6$, $y = +26$, $z = -10$ (Gutman et al., 2009) in MNI152 (2 mm) standard space in the left and right hemisphere as center points. The expanded ROI ($5 \times 5 \times 5$ voxels) was chosen to be purposefully generous and inclusive of the region described as SCC in the literature to account for interindividual anatomic variability in subsequent steps of analysis. These standard space masks were then transformed into the common structural space of the HCP dataset using the nonlinear transformation files provided by HCP (standard2acpc_dc) and nearest neighbor interpolation.

Subject-specific regions of interest: Using the atlas-defined left and right SCC seeds (Gutman et al., 2009), probabilistic tractography was performed with FDT in each subject's high-resolution T1 space (Behrens et al., 2003). Tractography parameters included 5,000 samples, 0.2 curvature threshold, loopcheck termination, 2,000 maximum number of steps, 0.5 mm step length and 0.01 subsidiary fiber fraction threshold using a whole brain target, and cerebrospinal fluid as an exclusion mask (80% threshold based on the maximum intensity value of the whole brain map). The whole brain tract map was then transformed to MNI152 space using nonlinear transformations provided by HCP (acpc_dc2standard) and nearest neighbor interpolation. To reduce the false positive connectivity voxels of the transformed maps, a low threshold (500) was applied in order to keep only those voxels with at least 500 streamlines from SCC.

Subject-specific white matter pathways were defined in a semi-automated fashion, using methods previously described (Tsolaki et al., 2017). For each tract or target region, we predefined larger regions of interest (illustrated in blue in Figure 1, Table 1). We then evaluated where each individual's whole brain SCC tract map intersected with these extended areas of interest in order to define subject-specific projection targets (illustrated in yellow in Figure 1). For each anatomically defined target, the coordinates of the voxel with maximum intensity value in the target area were used as a center point to create each subject-specific target mask (mPFC: $5 \times 5 \times 5$ voxel ROI, ACC: $5 \times 5 \times 5$ voxel ROI, UCF = $2 \times 2 \times 2$ voxel ROI and VS: voxel ROI in MNI_152 (2 mm); Figure 1iii).

2.3 | SCC to target probabilistic tractography

Using the same tractography parameters described above, probabilistic tractography was performed to estimate the ipsilateral connectivity from left and right SCC to VS, UCF, and ACC termination regions in both hemispheres, and to the left and right mPFC termination regions separately (SCC-to-mPFC connections include association as well as commissural pathways via the forceps minor). Each target mask was defined as a waypoint mask in order to discard tracts that do not pass through the target, a termination mask in order to terminate the pathways as soon as they enter the termination mask, and a classification mask in order to quantify connectivity values between the seed and target mask (Behrens et al., 2003).

To find the average SCC connectivity to each target region, each subject's probabilistic SCC map for each target was first registered nonlinearly to MNI152 space (acpc_dc2standard, nearest neighbor interpolation) and then divided by the total number of streamlines that were sent out from the seed. Finally, since the goal was to delineate the existence of connectivity between SCC and the targets without considering the strength of the connectivity, each SCC probabilistic map was normalized to have values between zero and one. An average probabilistic map for each target was then created across subjects. Finally, average SCC connectivity tracts to each target region were calculated across subjects. First, each tract map was divided by the total number of streamlines generated from the seed area and binarized at 0.005 threshold. Then the average fiber pathway to each target was calculated across all subjects.

2.4 | Defining the variability of the "tractography optimized target"

We define the "tractography optimized target" (TOT) within SCC as the subregion with the highest joint probability of connectivity with all four target areas (Tsolaki et al., 2017). First, the SCC probability maps for each target were smoothed using a Gaussian kernel (2 mm), multiplied on a voxel-by-voxel basis and then high pass filtered in order to include only voxels with probability higher than 10% of the maximum joint probability value. The voxel within TOT with the maximum joint probability of connectivity to all targets (TOT_Max) was identified in each subject.

2.5 | Statistical analysis

The variability in the spatial distributions of the voxel within SCC with maximum connectivity with each target was both visually and quantitatively assessed. Since the distributions were not symmetrical, the nonparametric Wilcoxon Signed-Rank test was used to assess pairwise differences in the distributions along each axis. The null hypothesis was that the difference between the pairs follows a symmetric distribution around zero. To correct for multiple comparisons, the Bonferroni correction was applied. The same approach was followed to evaluate the difference between the TOT_Max and the voxel with maximum probability of connectivity with each target within SCC.

3 | RESULTS

To evaluate the population-level probability of connectivity of each voxel in SCC to each of the four targets, we calculated voxel-by-voxel

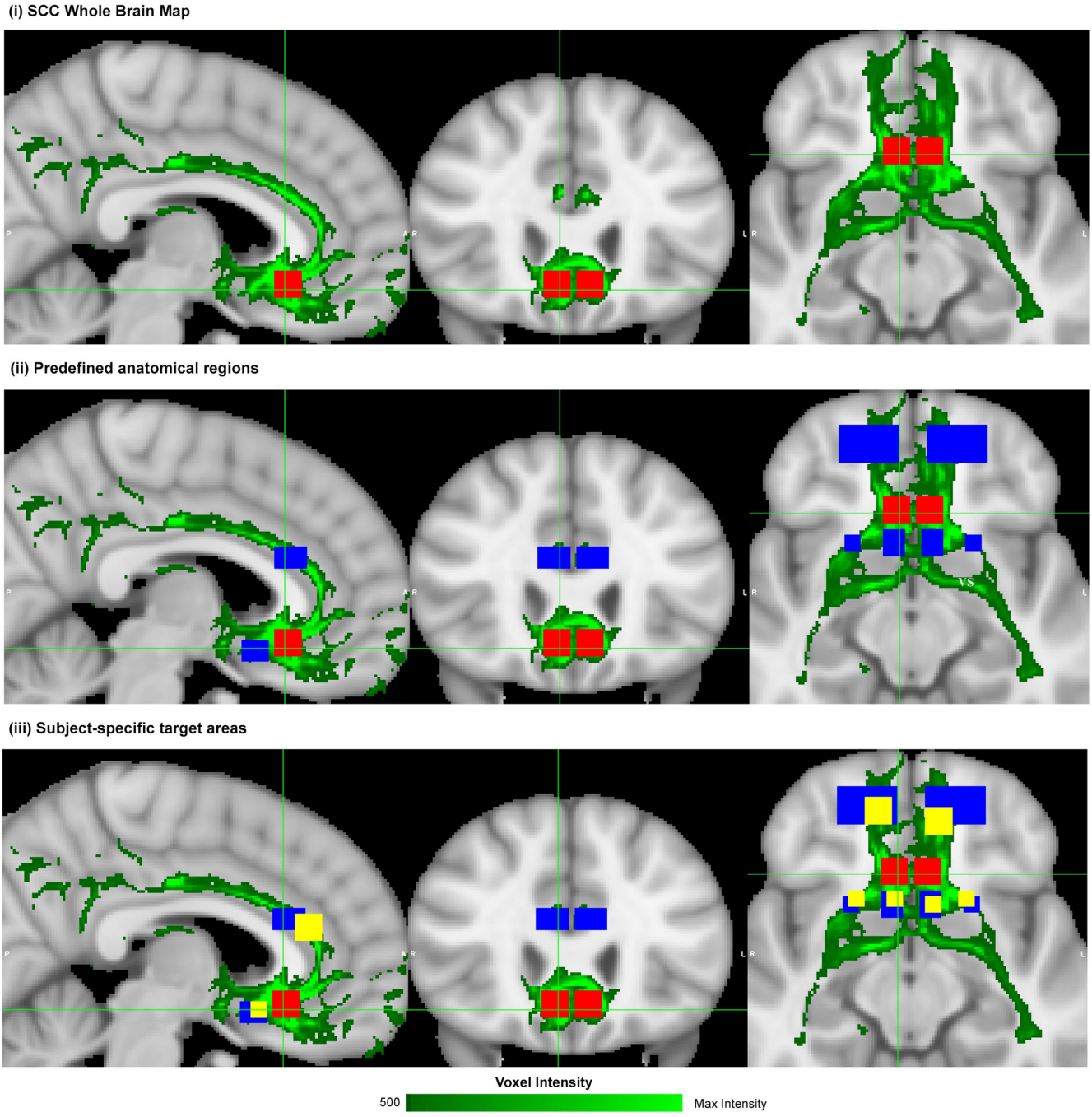

FIGURE 1 Subject-specific target identification. (i) The SCC (red masks) connectivity with the whole brain was delineated (green map). (ii) The major fiber pathways of forceps minor, uncinate fasciculus, cingulum and fronto-striatal bundles were identified to the resulted whole brain tractography map. Then, using predefined anatomical areas (blue masks) as identified by a neurosurgeon, that correspond to extended UCF, VS, ACC, and mPFC areas, the termination area of each fiber was determined to each predefined anatomical region. (iii) To each predefined area, the maximum intensity value of the voxel with the highest probability of connectivity within the area was determined and was used as center point to create subject-specific targets masks (yellow masks)

averages of target-specific probabilities across subjects in MNI space (Figure 2). For reference, the distribution of subject-specific target coordinates used for SCC mapping and segmentation are illustrated in Figure S1, highlighting variability in the target region between subjects and the rationale of using subject-specific targets. Four different connectivity patterns were identified in the group-level SCC segmentation maps for each target, with the voxels with highest probability of connectivity (probability >.8) delineated in yellow (Figure 2). Four patterns emerged: (a) SCC-UCF fibers are in the posterior-lateral area of the anatomically-defined SCC (b) SCC-VS fibers are also observed posteriorly, but more medially than SCC-UCF (c) SCC-ACC fibers originate in the superior-medial region of SCC (d) SCC-mPFC fibers center anteriolaterally. The voxels corresponding to the maximum probability of connectivity to each target are detailed in Table 2.

TABLE 1 The range of *X*, *Y*, and *Z* coordinate locations for each predefined region-of-interest

	UCF		VS		ACC		mPFC	
	L	R	L	R	L	R	L	R
X	−24:20	20:24	−8:−16	16:8	−2:−12	12:2	−6:−26	26:6
Y	12:16	12:16	6:12	6:12	22:34	22:34	44:56	44:56
Z	−16:−12	−16:−12	−12:−8	−12:−8	8:24	8:24	−12:4	−12:4

Note: The range of *X*, *Y*, and *Z* coordinate locations for each predefined region-of-interest (ROI) chosen based on termination points of the forceps minor, uncinate fasciculus, cingulum and fronto-striatal fiber bundles in MNI 152 standard space.

While the analyses displayed in Figure 2 illustrate the voxel-by-voxel distribution of connectivity probabilities to each of the four targets averaged across subjects, further analyses were conducted to assess the intersubject variability in the spatial distribution of probabilities (Figure 3). For each subject, we identified the voxel (in MNI space) with the maximum probability of connectivity and plotted histograms for each of the four targets (Figure 3). For example, for SCC-UCF, more than 80% of subjects were found to have maximum connectivity to UCF in the lateral aspect of SCC. The same pattern of skewness was observed in the SCC-mPFC maps for both hemispheres, with most subjects showing maximum connectivity in the lateral aspects of SCC. However, maximal mPFC connectivity was more frequently superior and anterior compared to the connectivity to the UCF target, where the SCC-UCF fibers were found in posterior regions of SCC. It is noteworthy that no single MNI coordinate accounted for more than 60% of the connectivity to any target across subjects. The average SCC tracts to each target for a single subject and across all the subjects are illustrated in Figure S2.

Although the TOT requires further clinical validation, we evaluated its variability as well. First, for each subject, we determined a voxel-wise joint probability of connectivity with all four targets and mapped these across subjects (Figure 4a). The voxels with the highest probability of joint connectivity were found in superior-lateral parts of SCC in left hemisphere and in superior but more medial parts of SCC in right hemisphere. To evaluate intersubject variability, we evaluated the TOT_max, or the single voxel (in MNI space) for each subject with the highest joint probability of connectivity with all four targets (Figure 4a, red-yellow overlay). The distribution of TOT_max voxels along the *x*, *y*, and *z* axes are depicted in Figure 4b. Along the *X* dimension, approximately 80 subjects were found to have TOT_max in the lateral region of SCC. Compared to the left hemisphere, TOT_Max was more medial in the right hemisphere. Along the *z* axis, the majority of subjects had maximum TOT connectivity in the superior part of SCC bilaterally (MNI coordinates: *X*-axis left/right hemisphere: mean = 99.1/83.0, *SD* = 0.7/1.1, median = 99.0/83.0, *Y*-axis left/right hemisphere mean = 152.3/152.9, *SD* = 2.0/1.9, median = 153.0/153.0, *Z*-axis left/right hemisphere mean = 64.8/64.9, *SD* = 1.1/1.3, median = 65.0/65.0). TOT_Max is located near the mean coordinates of the voxels with maximum connectivity within SCC (Table 3).

The spatial distributions of the voxel with maximum probability of connectivity to each of the four targets along the each *x*, *y*, and *z* axes were nearly all statistically different (p <.0001, Table 4). Only few pair comparisons failed to reject null hypothesis. Specifically, along the x axis, the comparison between SCC-UCF and SCC-mPFC in bilateral hemispheres (Z = −2.054, p = .040) and between SCC-mPFC_L and SCC-mPFC_R on the left hemisphere (Z = −5.44, p = .587) did not show significant differences. Along the *y* axis, right hemisphere SCC-UCF and SCC-VS (Z = −.442, p = .658) spatial distributions also did not differ. Finally, along the *z* axis, the comparison between SCC-ACC and SCC-mPFC_R were not significantly different in both hemispheres (left: Z = −.053, p = .958, right: Z = −.053, p = .958).

The same approach was followed to evaluate the difference between TOT_Max and SCC distributions for each target, demonstrating significant differences for all four targets for both hemispheres along the *x* axis (p <.00001). Along the y axis, the comparison between TOT_Max and SCC connectivity distributions to UCF, VS, and contralateral mPFC targets for both hemispheres rejected the hull hypothesis (p <.00001). Finally, the TOT_Max distribution along the *z* axis was significantly different compared to SCC connectivity distributions to UCF and VS and contralateral mPFC targets for both hemispheres. The Box plots (Figure 5) illustrate the pattern of symmetry across hemispheres and the degree of dispersion of each SCC and TOT_Max connectivity distribution. Of note, TOT_Max appears to be centered in the *x*-dimension, while being within or near the hotspots for mPFC and ACC in the *y* dimension and mPFC in the *z* dimension.

4 | DISCUSSION

In most but not all individuals, we identified four relatively subregions within the SCC, each with distinct connectivity patterns: a posterior-lateral region with connectivity to UCF, a posterior-medial region with connectivity to VS, a superior-medial region with connectivity to ACC and an anterior-lateral region with connectivity to mPFC. Characterization of the local architecture of SCC is important as it has been described as having significant variability and lacks clear anatomical landmarks that can be identified with routine in vivo structural/anatomic imaging (Riva-Posse et al., 2018). Previous studies were restricted to delineation of the structural connectivity of SCC with the whole brain (Gutman et al., 2009) or investigated the connectivity of SCC with areas with functional changes after DBS treatment (Johansen-Berg et al., 2007) without examining different connectivity patterns of subregions within the SCC. In this study, using data from

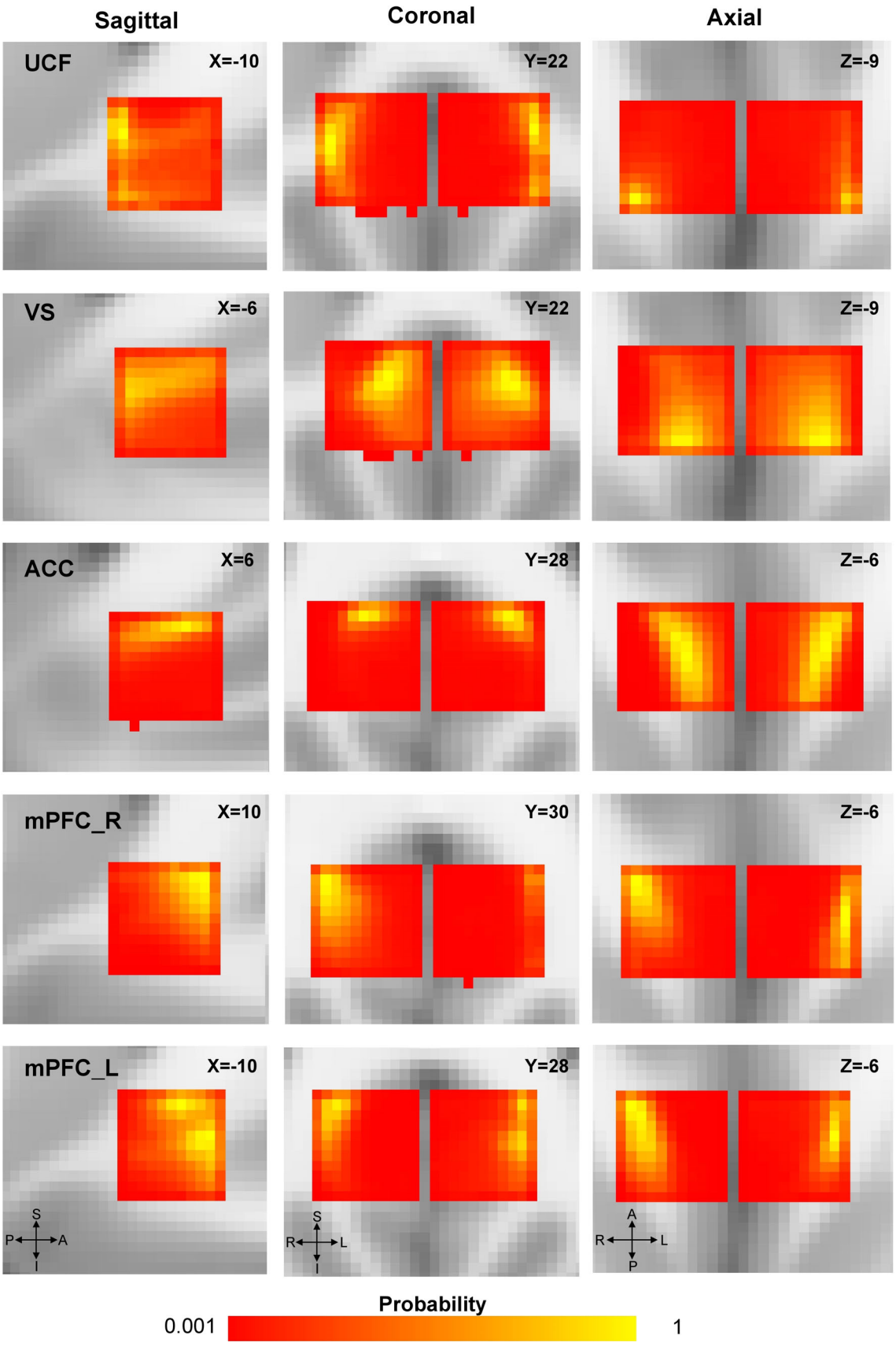

FIGURE 2 Legend on next page.

TABLE 2 Coordinates of voxels within SCC average maps that presented maximum probability of connectivity to each target

	UCF		VS		ACC		mPFC R		mPFC L	
	L	R	L	R	L	R	L	R	L	R
X	−10	10	−8	5	−8	5	−10	10	−10	10
Y	22	22	22	22	27	26	26	30	27	30
Z	−8	−9	−9	−8	−6	−6	−6	−6	−6	−6

Note: MNI152 coordinates of the voxels within average SCC probabilistic maps to UCF, VS, ACC, and mPFC that sent out the maximum number of fibers to each ROI.

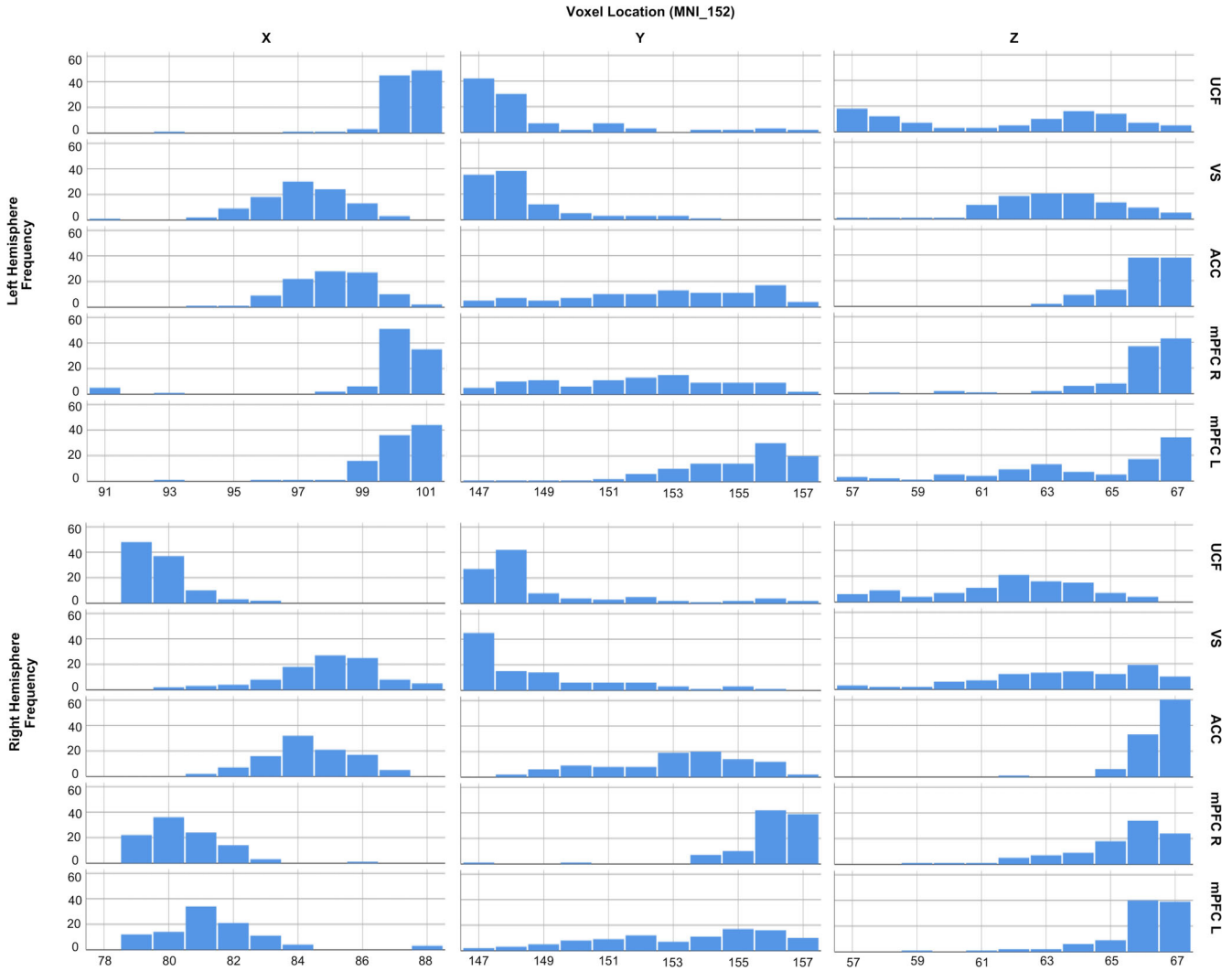

FIGURE 3 Distribution of maximum SCC connectivity across subjects. *X*, *Y*, and *Z* coordinates of maximum connectivity voxel within SCC probabilistic maps: The histogram distribution displayed differences in SCC probabilistic maps (blue histograms) to each target. Across subjects the areas within SCC with the maximum number of streamlines were found posterior-lateral for SCC-UCF, posterior-medial for SCC-VS, superior-medial for SCC-ACC map, and anterior-lateral for SCC-mPFC maps

FIGURE 2 Average SCC probabilistic maps and distribution of connectivity across subjects. To calculate the average SCC probabilistic map to each target, first each SCC map was divided by the total number of streamlines that were sent out from the seed and then normalized to have values between zero and one in order to highlight the connectivity to the target area. Finally, to evaluate the population-level probability of connectivity of each voxel in SCC to each of the four targets, we calculated voxel-by-voxel averages of target-specific probabilities across the 100 subjects in MNI space The resulted SCC topographic maps to UCF, VS, ACC, and mPFC presented distinct connectivity patterns to each target. SCC-UCF map's region that sent out the maximum number of streamlines was found in the posterior-lateral area of SCC. SCC-VS fibers were also observed posteriorly, but more medially compared to SCC-UCF map. SCC-ACC fibers originated in the superior-medial region of SCC, while SCC-mPFC fibers centered anterolaterally. The voxels (yellow color) of SCC maps with higher probability of connectivity (probability >.8) to UCF, VS, ACC and mPFC were overlaid on the segmentation maps

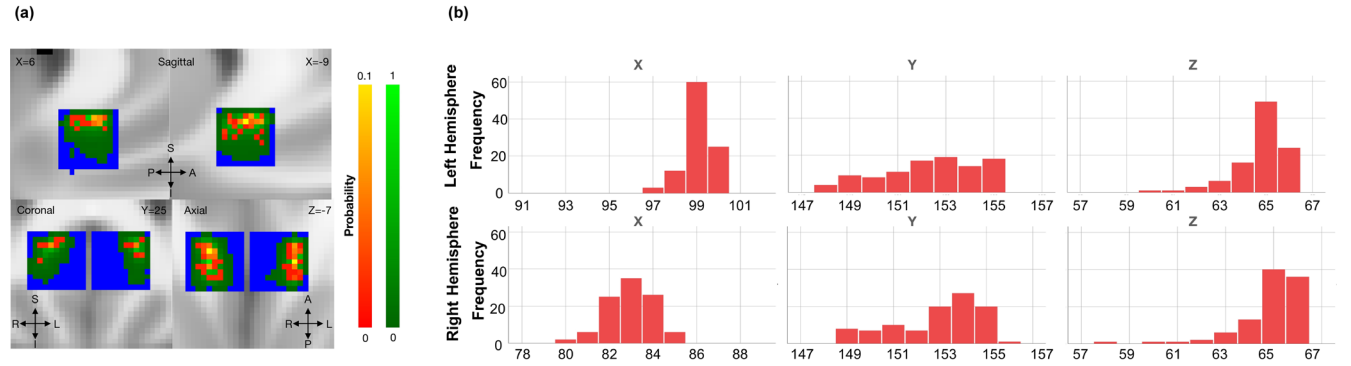

FIGURE 4 Tractography optimized target and distribution of connectivity across subjects. (a) TOT Average Probabilistic Map: The TOT maps present highest probability of connectivity within the superior-lateral parts of SCC with a variability between 1 and 8 mm along the y axis. The voxels (red-yellow color) with higher probability of connectivity within TOT (TOT_Max) were overlaid on the average TOT maps. (b)The distribution of the coordinates of the voxels within TOT that presented maximum connectivity to all four subject-specific targets (red histograms) (TOT Max) presented the variance on the coordinates within the hot-spot area. The distribution showed that the majority of the subjects presented TOT_Max within the superior-lateral (left hemisphere) and medial (right hemisphere) parts of SCC

TABLE 3 Mean *X*, *Y*, and *Z* coordinates of voxels with maximum connectivity within SCC probabilistic maps and within TOT

		Coordinates MNI 152		
	ROI	*X*	*Y*	*Z*
Left hemisphere	UCF	100.3 ± 1.0	148.7 ± 2.5	61.7 ± 3.4
	VS	97.1 ± 1.5	148.3 ± 1.6	63.4 ± 1.9
	ACC	98.1 ± 1.3	152.6 ± 2.9	66.0 ± 1.0
	mPFC R	100.1 ± 2.2	151.9 ± 2.7	65.9 ± 1.6
	mPFC L	100.1 ± 1.2	154.8 ± 2.1	64.4 ± 2.8
	TOT_Max	99.1 ± 0.7	152.3 ± 2.0	64.8 ± 1.1
Right hemisphere	UCF	79.7 ± 0.9	149.0 ± 2.6	61.8 ± 2.4
	VS	84.9 ± 1.7	148.7 ± 2.3	63.6 ± 2.6
	ACC	84.3 ± 1.4	153.1 ± 2.2	66.5 ± 0.8
	mPFC R	80.5 ± 1.2	156.0 ± 1.4	65.3 ± 1.7
	mPFC L	81.5 ± 1.9	153.3 ± 2.7	65.9 ± 1.4
	TOT_Max	83.0 ± 1.1	152.9 ± 1.9	64.9 ± 1.3

Note: The mean values (standard deviation) of the maximum connectivity voxels was calculated. A variability between 1 and 3 mm was observed across subjects with respect to the maximum connectivity area within SCC. For both hemispheres, the TOT is located around the mean values of the *X*, *Y*, and *Z* coordinates of the voxels of maximum connectivity within SCC.

the Human Connectome Project, we provide a more comprehensive group-level characterization of the general patterns of connectivity of SCC to areas critical to depression (Riva-Posse et al., 2014). Importantly, there is a symmetry across hemispheres of the location of maximum SCC connectivity for most targets with the exception of ACC and mPFC targets. This asymmetry may be due to higher intrinsic variability of connectivity of these areas since these tracts are responsible for the most variability in targeting.

Despite some consistency in the patterns of white matter connectivity in SCC, perhaps equally important is the variability of the underlying anatomy. The voxel within SCC with maximum connectivity to each target varied with a standard deviation of 1–3 mm across subjects (Table 3). Furthermore, not a single voxel in MNI space accounted for more than 60% of the connectivity for any target. This variability highlights differences in interindividual anatomy and potentially can have important implications for therapeutic translation. The long-tailed distributions and the difference of SCC connectivity pattern between the hemispheres suggest an inherent sensitivity of spatial positioning with the proposed model of targeting.

The findings of the current study are of potential clinical interest in refining the targeting for SCC DBS. Despite the promising results of SCC DBS, the best stimulation target within SCC is still an open issue that requires further investigation. In the first open label studies, the most efficacious targets were localized to the gray-white matter junction close to Broadman area 25 (Lozano et al., 2008, 2011; Mayberg et al., 2005). Studies trying to associate the anatomical position of the lead placement with effective clinical outcome found no differences between responders and nonresponders (Hamani et al., 2009; Lozano

TABLE 4 Comparison of the medians of SCC and TOT_Max connectivity distributions along *x*,*y*, and *z* axes

P Wilcoxon Sign Rank Test

		Right Hemisphere					
		UCF	VS	ACC	mPFC R	mPFC L	TOT
X	Left Hemisphere						
	UCF		0.000	0.000	0.000	0.000	0.000
	VS	0.000		0.002	0.000	0.000	0.000
	ACC	0.000	0.000		0.000	0.000	0.000
	mPFC R	0.014	0.000	0.000		0.000	0.000
	mPFC L	0.040	0.000	0.000	0.587		0.000
	TOT	0.000	0.000	0.000	0.000	0.000	
Y	Left Hemisphere						
	UCF		0.658	0.000	0.000	0.000	0.000
	VS	0.869		0.000	0.000	0.000	0.000
	ACC	0.000	0.000		0.000	0.594	0.429
	mPFC R	0.000	0.000	0.056		0.000	0.000
	mPFC L	0.000	0.000	0.000	0.000		0.112
	TOT	0.000	0.000	0.186	0.179	0.000	
Z	Left Hemisphere						
	UCF		0.000	0.000	0.000	0.000	0.000
	VS	0.000		0.000	0.000	0.003	0.000
	ACC	0.000	0.000		0.958	0.000	0.000
	mPFC R	0.000	0.000	0.958		0.000	0.000
	mPFC L	0.000	0.003	0.000	0.000		0.199
	TOT	0.000	0.000	0.000	0.000	0.475	

Z Wilcoxon Sign Rank Test

		Right Hemisphere					
		UCF	VS	ACC	mPFC R	mPFC L	TOT
X	Left Hemisphere						
	UCF		-8.720	-8.680	-4.688	-6.540	-8.755
	VS	-8.373		-3.162	-8.533	-7.655	-7.421
	ACC	-8.038	-4.823		-8.594	-7.367	-7.097
	mPFC R	-2.461	-6.868	-6.204		-4.316	-8.260
	mPFC L	-2.054	-8.224	-7.672	-0.544		-6.256
	TOT	-7.736	-8.292	-6.446	-5.607	-6.637	
Y	Left Hemisphere						
	UCF		-0.442	-7.488	-8.447	-7.374	-7.323
	VS	-0.165		-7.800	-8.543	-7.723	-8.107
	ACC	-7.555	-8.128		-7.536	-0.533	-0.791
	mPFC R	-6.480	-7.420	-1.912		-6.970	-7.845
	mPFC L	-8.357	-8.572	-5.132	-6.543		-1.591
	TOT	-7.689	-8.216	-1.322	-1.344	-6.882	
Z	Left Hemisphere						
	UCF		-3.775	-8.064	-7.779	-5.561	-6.978
	VS	-3.775		-8.005	-7.149	-2.983	-5.480
	ACC	-8.064	-8.005		-0.053	-4.883	-6.421
	mPFC R	-7.779	-7.149	-0.053		-4.824	-5.561
	mPFC L	-5.561	-2.983	-4.883	-4.824		-1.283
	TOT	-6.781	-5.765	-6.826	-5.856	-0.714	

Smaller — Higher

Marginal Difference

Note: Wilcoxon Signed-Rank test was used to assess whether the medians of SCC and TOT_Max distributions of maximum probabilities to the four targets along the each *x*, *y*, and *z* axes were different. The results indicated that overall the null hypothesis was rejected indicating that the medians of the pair distributions were different along the axes for each *X*, *Y*, and *Z* coordinate (p <.0033 after Bonferroni correction). The green cells delineate the pair comparisons that failed to reject null hypothesis indicating that the two medians were the same. The *Z* values that correspond to the magnitude of difference between the medians of the pair distributions are illustrated on the table with blue color. The lighter blue corresponds to larger difference while darker blue corresponds to smaller difference between the median of the pair distributions.

et al., 2012). Still, subsequent studies have identified some putative imaging biomarkers of successful SCC DBS. In one such study the best stimulation area includes a cluster in the vicinity of the lateral border of the SCC approximately 7 mm lateral to the midline and 4 mm ventral to the corpus callosum (Merkl et al., 2013). In another, where a sham controlled discontinuation phase was used, a long-term response was observed when the stimulation site was closer to Broadman area 24 (Puigdemont et al., 2015). The results of the current study might contribute to the optimization of SCC DBS target identification based on structural anatomy and connectivity. The calculation of the average TOT maps across subjects highlights that the TOT, as previously defined, is most often in the superior-lateral and superior- medial aspects of the SCC. However, the variability that was observed along the *x* (right hemisphere) and *y* (bilaterally) axes suggests that group-level coordinates of hot spots should not be used for individual targeting since there is a different structural connectivity pattern based on subject-specific anatomy.

Given the network-basis of depression, the optimal DBS target likely involves the convergence of white matter tracts implicated in multiple key disease-related circuits (Accolla et al., 2016; Lujan et al., 2012; Riva-Posse et al., 2018). However, this tractography approach has not been validated beyond a single institution (Riva-Posse et al., 2018) and it is based on iterative deterministic assessments, which is prone to sampling limitations (Petersen et al., 2016). In the current study a data-driven automated method for the definition of the TOT area was used based on probabilistic approach. However, probabilistic tractography is time consuming, its data-driven nature may provide a better practical approach in delineation of individualized anatomy over deterministic, tends to capture more disperse trajectories than deterministic methods and may delineate more functionally distinct fiber pathways (Behrens et al., 2003). To our knowledge, a data-driven automated approach to define the optimal target and provide a tomographic (visual) map to guide targeting does not exist. This method could be used clinically in an intuitive fashion for DBS targeting and programming. Finally, an interested follow up study would be to compare TOT in a blind way with the DBS SCC target area that was used in other centers and associate the results with clinical outcome.

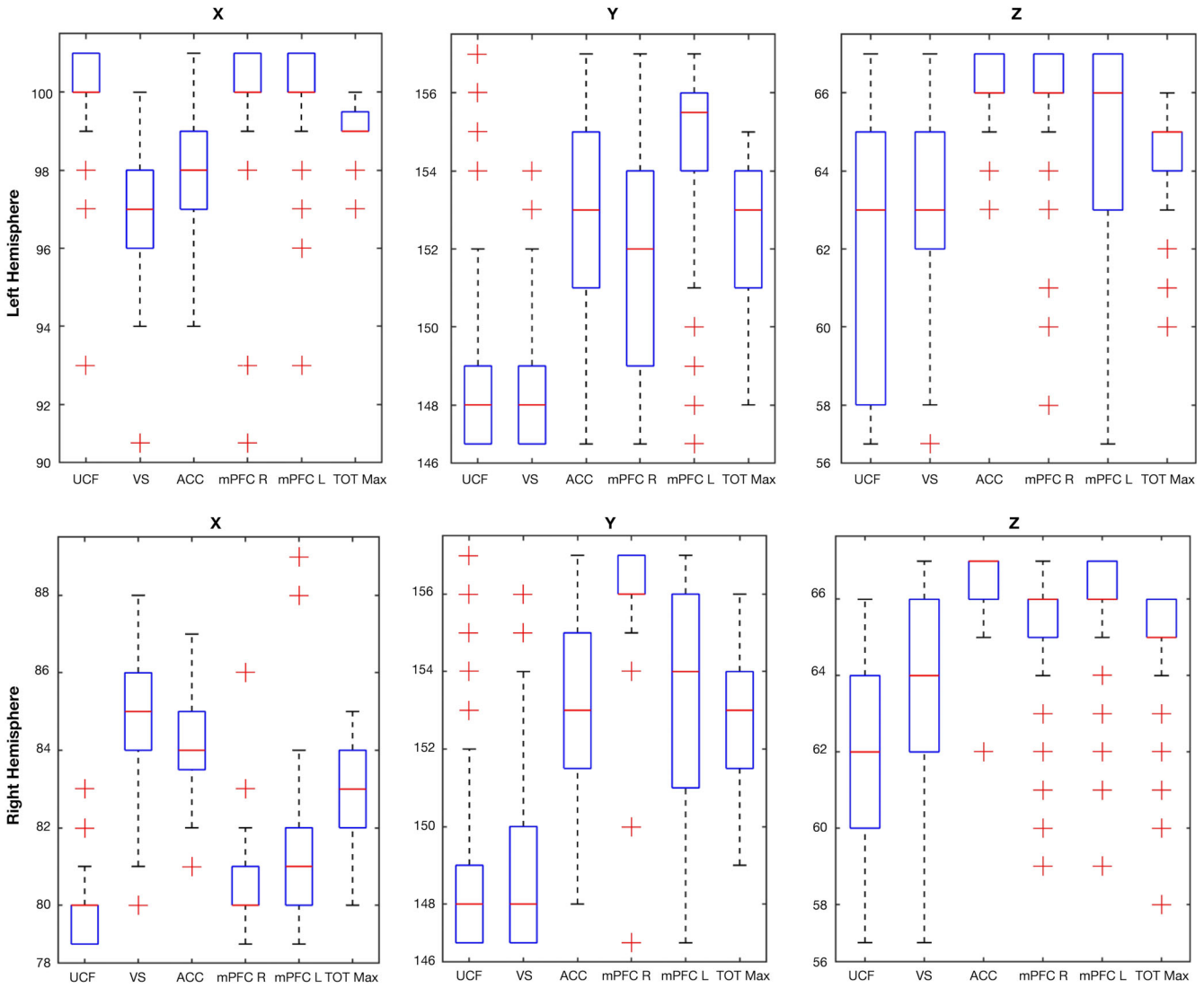

FIGURE 5 Box plots of the SCC and TOT_Max connectivity distributions along *x*,*y*, and *z* axes. The Box plots illustrate the pattern of symmetry and asymmetry across hemispheres and the degree of dispersion of each SCC and TOT_Max connectivity distribution

Despite having implications for targeting DBS for TRD, the current study evaluated healthy subjects from the HCP. While these are two different populations, we note that while the integrity of white matter tracts can change with disease (and disease severity), disease does not eliminate or lead to structural rearrangement of white matter tracts. Therefore, the overall spatial pattern of white matter tracts, even in healthy subjects, is still relevant and useful to study.

The identification of the optimal tracts to be targeted is still under investigation with studies suggesting involvement of UCF, FM, and cingulum bundles with improved acute intraoperative behavior responses (Choi et al., 2015) and direct activation of right CB, left CB, and FM pathways may be the most likely therapeutic targets for SCC targets (Howell et al., 2019). The optimal pattern of white matter bundle targeting and stimulation may ultimately depend on the constellation of symptoms. A recent study reported positive results of SCC DBS in treatment of PTSD, noting that involvement of UCF appears to have more important role in this disorder than in depression (Hamani et al., 2020). While further work is needed to define the optimal white matter stimulation pattern, understanding the underlying anatomy and intersubject variability still informs future approaches to interventions. In the current study, the use of healthy subjects does not allow the evaluation of clinical value of each of these white matter pathways. Future studies should investigate the structural (and functional) SCC connectivity to each target area in association with the clinical outcome, and also the relationship between functional and structural SCC connectivity. The reliability of the current results should be investigated in future studies using cross validation using a larger sample of subjects.

Regarding the methodology employed for tractography, there is a controversy regarding which diffusion tractography analytic approach is more reliable for reproducing known anatomy, with results highly dependent on data quality, the algorithm selected, and the parameter settings (Knösche, Anwander, Liptrot, & Dyrby, 2015; Thomas et al.,

2014). Deterministic tractography is a fast approach, but is characterized by increased uncertainty in dense areas and is prone to sampling limitations (Avecillas-Chasin, Alonso-Frech, Parras, del Prado, & Barcia, 2015). The probabilistic approach on the other hand is computationally demanding and time intensive compared to deterministic and it can be more sensitive to nondominant fiber pathways and more prone to false positives (Johansen-Berg et al., 2007). Probabilistic tractography considers intravoxel crossing fibers (Behrens, Berg, Jbabdi, Rushworth, & Woolrich, 2007) and estimates the pathways that originate at any given seed voxel. For the questions posed here, the current study shows the specific value of the probabilistic approach to explore intersubject consistency and variability in subregional white matter anatomy. However, its data-driven nature may provide a better practical approach in delineation of individualized anatomy over deterministic, tends to capture more disperse trajectories than deterministic methods and may delineate more functionally distinct fiber pathways (Behrens et al., 2003).

5 | CONCLUSIONS

Probabilistic tractography-based parcellation of SCC revealed four distinct connectivity regions within the SCC, with relative constancy across individuals but still with notable variability. Understanding the pattern of fiber organization within SCC is important to understanding the anatomic organization of the brain as well as advancing therapeutic interventions using network-based approaches. Using patient-specific methods to define connectivity patterns, as done here, may be important to understanding the connectivity-based anatomy and organization of other brain regions.

CONFLICT OF INTEREST

The authors declare no potential conflict of interest.

DATA AVAILABILITY STATEMENT

Diffusion and structural 3T data from 100 healthy subjects from the "WU-Minn HCP Data—1200 Subjects" public dataset of the Human Connectome Project (http://www.humanconnectome.org/; Van Essen et al., 2013) were used for this study due to the high quality, superior spatial resolution, and validated nature of this dataset.

ORCID

Evangelia Tsolaki https://orcid.org/0000-0002-8333-9493
Nader Pouratian https://orcid.org/0000-0002-0426-3241

REFERENCES

Accolla, E. A., Aust, S., Merkl, A., Schneider, G.-H., Kühn, A. A., Bajbouj, M., & Draganski, B. (2016). Deep brain stimulation of the posterior gyrus rectus region for treatment resistant depression. *Journal of Affective Disorders*, *194*, 33–37. http://www.sciencedirect.com/science/article/pii/S016503271530536X

Argyelan, M., Lencz, T., Kaliora, S., Sarpal, D. K., Weissman, N., Kingsley, P. B., … Petrides, G. (2016). Subgenual cingulate cortical activity predicts the efficacy of electroconvulsive therapy. *Translational Psychiatry*, *6*, e789–e789. https://www.ncbi.nlm.nih.gov/pubmed/27115120

Avecillas-Chasin, J. M., Alonso-Frech, F., Parras, O., del Prado, N., & Barcia, J. A. (2015). Assessment of a method to determine deep brain stimulation targets using deterministic tractography in a navigation system. *Neurosurgical Review*, *38*, 739–751. https://doi.org/10.1007/s10143-015-0643-1

Behrens, T. E. J., Berg, H. J., Jbabdi, S., Rushworth, M. F. S., & Woolrich, M. W. (2007). Probabilistic diffusion tractography with multiple fibre orientations: What can we gain? *NeuroImage*, *34*, 144–155. http://www.sciencedirect.com/science/article/pii/S1053811906009360

Behrens, T. E. J., Woolrich, M. W., Jenkinson, M., Johansen-Berg, H., Nunes, R. G., Clare, S., … Smith, S. M. (2003). Characterization and propagation of uncertainty in diffusion-weighted MR imaging. *Magnetic Resonance in Medicine*, *50*, 1077–1088.

Bhatia, K. D., Henderson, L. A., Hsu, E., & Yim, M. (2018). Reduced integrity of the uncinate fasciculus and cingulum in depression: A stem-by-stem analysis. *Journal of Affective Disorders*, *235*, 220–228. http://www.sciencedirect.com/science/article/pii/S0165032718303951

Choi, K. S., Riva-Posse, P., Gross, R. E., & Mayberg, H. S. (2015). Mapping the 'depression switch' during intraoperative testing of subcallosal cingulate deep brain stimulation. *JAMA Neurology*, *72*, 1252–1260.

Dougherty, D. D., Weiss, A. P., Cosgrove, G. R., Alpert, N. M., Cassem, E. H., Nierenberg, A. A., … Rauch, S. L. (2003). Cerebral metabolic correlates as potential predictors of response to anterior cingulotomy for treatment of major depression. *Journal of Neurosurgery*, *99*, 1010–1017. https://doi.org/10.3171/jns.2003.99.6.1010

Drevets, W. C., Price, J. L., & Furey, M. L. (2008). Brain structural and functional abnormalities in mood disorders: Implications for neurocircuitry models of depression. *Brain Structure & Function*, *213*, 93–118.

Drevets, W. C., Savitz, J., & Trimble, M. (2008). The subgenual anterior cingulate cortex in mood disorders. *CNS Spectrums*, *13*, 663–681. https://www.ncbi.nlm.nih.gov/pubmed/18704022

Goldapple, K., Segal, Z., Garson, C., & Lau, M. (2004). Modulation of cortical-limbic pathways in major depression:Treatment-specific effects of cognitive behavior therapy. *Archives of General Psychiatry*, *61*, 34–41.

Gutman, D. A., Holtzheimer, P. E., Behrens, T. E. J., Johansen-Berg, H., & Mayberg, H. S. (2009). A Tractography analysis of two deep brain stimulation white matter targets for depression. *Biological Psychiatry*, *65*, 276–282.

Hamani, C., Davidson, B., Levitt, A., Meng, Y., Corchs, F., Abrahao, A., …, Lipsman, N. (2020). Patient with posttraumatic stress disorder successfully treated with deep brain stimulation of the medial prefrontal cortex and uncinate fasciculus. *Biological Psychiatry*. https://doi.org/10.1016/j.biopsych.2020.05.018

Hamani, C., Mayberg, H., Snyder, B., Giacobbe, P., Kennedy, S., & Lozano, A. M. (2009). Deep brain stimulation of the subcallosal cingulate gyrus for depression: Anatomical location of active contacts in clinical responders and a suggested guideline for targeting. *Journal of Neurosurgery*, *111*, 1209–1215. https://doi.org/10.3171/2008.10.JNS08763

Hamani, C., Mayberg, H., Stone, S., Laxton, A., Haber, S., & Lozano, A. M. (2011). The subcallosal cingulate gyrus in the context of major depression. *Biological Psychiatry*, *69*, 301–308. https://doi.org/10.1016/j.biopsych.2010.09.034

Holtzheimer, P. E., Kelley, M. E., Gross, R. E., Filkowski, M. M., Garlow, S. J., Barrocas, A., … Mayberg, H. S. (2012). Subcallosal cingulate deep brain stimulation for treatment-resistant unipolar and bipolar depression. *Archives of General Psychiatry*, *69*, 150–158. http://www.ncbi.nlm.nih.gov/pmc/articles/PMC4423545/

Howell, B., Choi, K. S., Gunalan, K., Rajendra, J., Mayberg, H. S., & McIntyre, C. C. (2019). Quantifying the axonal pathways directly

stimulated in therapeutic subcallosal cingulate deep brain stimulation. *Human Brain Mapping*, *40*, 889–903.

Izuma, K., Saito, D. N., & Sadato, N. (2008). Processing of social and monetary rewards in the human striatum. *Neuron*, *58*, 284–294.

Johansen-Berg, H., Rushworth, M. F. S., Behrens, T. E. J., Matthews, P. M., Gutman, D. A., Katz, E., … Lozano, A. M. (2007). Anatomical connectivity of the Subgenual cingulate region targeted with deep brain stimulation for treatment-resistant depression. *Cerebral Cortex*, *18*, 1374–1383.

Johnstone, T., van Reekum, C. M., Urry, H. L., Kalin, N. H., & Davidson, R. J. (2007). Failure to regulate: Counterproductive recruitment of top-down prefrontal-subcortical circuitry in major depression. *The Journal of Neuroscience*, *27*, 8877 LP–8884. http://www.jneurosci.org/content/27/33/8877.abstract

Jones, D. K., Christiansen, K. F., Chapman, R. J., & Aggleton, J. P. (2013). Distinct subdivisions of the cingulum bundle revealed by diffusion MRI fibre tracking: Implications for neuropsychological investigations. *Neuropsychologia*, *51*, 67–78. https://www.ncbi.nlm.nih.gov/pubmed/23178227

Kennedy, S. H., Konarski, J. Z., Segal, Z. V., Lau, M. A., Bieling, P. J., McIntyre, R. S., & Mayberg, H. S. (2007). Differences in brain glucose metabolism between responders to CBT and venlafaxine in a 16-week randomized controlled trial. *The American Journal of Psychiatry*, *164*, 778–788.

Knösche, T. R., Anwander, A., Liptrot, M., & Dyrby, T. B. (2015). Validation of tractography: Comparison with manganese tracing. *Human Brain Mapping*, *36*, 4116–4134. http://www.pubmedcentral.nih.gov/articlerender.fcgi?artid=5034837&tool=pmcentrez&rendertype=abstract

Lozano, A. M., Giacobbe, P., Hamani, C., Rizvi, S. J., Kennedy, S. H., Kolivakis, T. T., … Mayberg, H. S. (2011). A multicenter pilot study of subcallosal cingulate area deep brain stimulation for treatment-resistant depression. *Journal of Neurosurgery*, *116*, 315–322. https://doi.org/10.3171/2011.10.JNS102122

Lozano, A. M., Mayberg, H. S., Giacobbe, P., Hamani, C., Craddock, R. C., & Kennedy, S. H. (2008). Subcallosal cingulate gyrus deep brain stimulation for treatment-resistant depression. *Biological Psychiatry*, *64*, 461–467. http://www.sciencedirect.com/science/article/pii/S0006322308007038

Lujan, J. L., Chaturvedi, A., Choi, K. S., Holtzheimer, P. E., Gross, R. E., Mayberg, H. S., & McIntyre, C. C. (2013). Tractography-activation models applied to subcallosal cingulate deep brain stimulation. *Brain Stimulation*, *6*, 737–739.

Lujan, J. L., Chaturvedi, A., Malone, D. A., Rezai, A. R., Machado, A. G., & McIntyre, C. C. (2012). Axonal pathways linked to therapeutic and nontherapeutic outcomes during psychiatric deep brain stimulation. *Human Brain Mapping*, *33*, 958–968.

Mayberg, H. S. (2003). Modulating dysfunctional limbic-cortical circuits in depression: Towards development of brain-based algorithms for diagnosis and optimised treatment. *British Medical Bulletin*, *65*, 193–207.

Mayberg, H. S. (2009). Targeted electrode-based modulation of neural circuits for depression. *The Journal of Clinical Investigation*, *119*, 717–725.

Mayberg, H. S., Brannan, S. K., Tekell, J. L., Silva, J. A., Mahurin, R. K., McGinnis, S., & Jerabek, P. A. (2000). Regional metabolic effects of fluoxetine in major depression: Serial changes and relationship to clinical response. *Biological Psychiatry*, *48*, 830–843. http://www.ncbi.nlm.nih.gov/pubmed/11063978

Mayberg, H. S., Liotti, M., Brannan, S. K., McGinnis, S., Mahurin, R. K., Jerabek, P. A., … Fox, P. T. (1999). Reciprocal limbic-cortical function and negative mood: Converging PET findings in depression and normal sadness. *The American Journal of Psychiatry*, *156*, 675–682.

Mayberg, H. S., Lozano, A. M., Voon, V., McNeely, H. E., Seminowicz, D., Hamani, C., … Kennedy, S. H. (2005). Deep brain stimulation for treatment-resistant depression. *Neuron*, *45*, 651–660. http://www.sciencedirect.com/science/article/pii/S089662730500156X

Merkl, A., Schneider, G. H., Schönecker, T., Aust, S., Kühl, K. P., Kupsch, A., … Bajbouj, M. (2013). Antidepressant effects after short-term and chronic stimulation of the subgenual cingulate gyrus in treatment-resistant depression. *Experimental Neurology*, *249*, 160–168. https://doi.org/10.1016/j.expneurol.2013.08.017

Mottaghy, F. M., Keller, C. E., Gangitano, M., Ly, J., Thall, M., Parker, J. A., & Pascual-Leone, A. (2002). Correlation of cerebral blood flow and treatment effects of repetitive transcranial magnetic stimulation in depressed patients. *Psychiatry Research*, *115*, 1–14.

Neimat, J. S., Hamani, C., Giacobbe, P., Merskey, H., Kennedy, S. H., Mayberg, H. S., & Lozano, A. M. (2008). Neural stimulation successfully treats depression in patients with prior ablative cingulotomy. *The American Journal of Psychiatry*, *165*, 687–693.

Nestler, E. J., Barrot, M., DiLeone, R. J., Eisch, A. J., Gold, S. J., & Monteggia, L. M. (2002). Neurobiology of depression. *Neuron*, *34*, 13–25. http://www.sciencedirect.com/science/article/pii/S0896627302006530

Nobler, M. S., Oquendo, M. A., Kegeles, L. S., Malone, K. M., Campbell, C., Sackeim, H. A., & Mann, J. J. (2001). Decreased regional brain metabolism after ECT. *The American Journal of Psychiatry*, *158*, 305–308.

Nobler, M. S., Teneback, C. C., Nahas, Z., Bohning, D. E., Shastri, A., Kozel, F. A., & George, M. S. (2000). Structural and functional neuroimaging of electroconvulsive therapy and transcranial magnetic stimulation. *Depression and Anxiety*, *12*, 144–156.

Olson, I. R., Der, H. R. J. V., Alm, K. H., & Vyas, G. (2015). Development of the uncinate fasciculus: Implications for theory and developmental disorders. *Developmental Cognitive Neuroscience*, *14*, 50–61.

Pardo, J. V., Sheikh, S. A., Schwindt, G. C., Lee, J. T., Kuskowski, M. A., Surerus, C., … Rittberg, B. R. (2008). Chronic vagus nerve stimulation for treatment-resistant depression decreases resting ventromedial prefrontal glucose metabolism. *NeuroImage*, *42*, 879–889. http://www.ncbi.nlm.nih.gov/pmc/articles/PMC2601663/

Petersen, M. V., Lund, T. E., Sunde, N., Frandsen, J., Rosendal, F., Juul, N., & Østergaard, K. (2016). Probabilistic versus deterministic tractography for delineation of the cortico-subthalamic hyperdirect pathway in patients with Parkinson disease selected for deep brain stimulation. *Journal of Neurosurgery*, *126*, 1–12. https://doi.org/10.3171/2016.4.JNS1624

Phillips, M. L. (2003). Understanding the neurobiology of emotion perception: Implications for psychiatry. *The British Journal of Psychiatry*, *182*, 190–192.

Puigdemont, D., Pérez-Egea, R., Portella, M. J., Molet, J., de Diego-Adeliño, J., Gironell, A., … Pérez, V. (2012). Deep brain stimulation of the subcallosal cingulate gyrus: Further evidence in treatment-resistant major depression. *The International Journal of Neuropsychopharmacology*, *15*, 121–133. https://doi.org/10.1017/S1461145711001088

Puigdemont, D., Portella, M. J., Pérez-Egea, R., Molet, J., Gironell, A., de Diego-Adeliño, J., … Pérez, V. (2015). A randomized double-blind crossover trial of deep brain stimulation of the subcallosal cingulate gyrus in patients with treatment-resistant depression: a pilot study of relapse prevention. *Journal of Psychiatry & Neuroscience*, *40*, 224–231. http://www.ncbi.nlm.nih.gov/pmc/articles/PMC4478055/

Riva-Posse, P., Choi, K. S., Holtzheimer, P. E., Crowell, A. L., Garlow, S. J., Rajendra, J. K., … Mayberg, H. S. (2018). A connectomic approach for subcallosal cingulate deep brain stimulation surgery: Prospective targeting in treatment-resistant depression. *Molecular Psychiatry*, *23*, 843–849. https://www.ncbi.nlm.nih.gov/pubmed/28397839

Riva-Posse, P., Choi, K. S., Holtzheimer, P. E., McIntyre, C. C., Gross, R. E., Chaturvedi, A., … Mayberg, H. S. (2014). Defining critical white matter pathways mediating successful subcallosal cingulate deep brain stimulation for treatment-resistant depression. *Biological Psychiatry*, *76*, 963–969. http://www.sciencedirect.com/science/article/pii/S0006322314002443

Seminowicz, D. A., Mayberg, H. S., McIntosh, A. R., Goldapple, K., Kennedy, S., Segal, Z., & Rafi-Tari, S. (2004). Limbic-frontal circuitry in major depression: A path modeling metanalysis. *NeuroImage*, *22*, 409–418.

Siegle, G. J., Carter, C. S., & Thase, M. E. (2006). Use of fMRI to predict recovery from unipolar depression with cognitive behavior therapy. *The American Journal of Psychiatry*, *163*, 735–738. https://doi.org/10.1176/ajp.2006.163.4.735.

Simmonds, D. J., Hallquist, M. N., Asato, M., & Luna, B. (2014). Developmental stages and sex differences of white matter and behavioral development through adolescence: A longitudinal diffusion tensor imaging (DTI) study. *NeuroImage*, *92*, 356–368. https://doi.org/10.1016/j.neuroimage.2013.12.044

Thomas, C., Ye, F. Q., Irfanoglu, M. O., Modi, P., Saleem, K. S., Leopold, D. A., & Pierpaoli, C. (2014). Anatomical accuracy of brain connections derived from diffusion MRI tractography is inherently limited. *Proceedings of the National Academy of Sciences*, *111*, 16574–16579. http://www.pnas.org/content/111/46/16574.abstract

Tsolaki, E., Espinoza, R., & Pouratian, N. (2017). Using probabilistic tractography to target the subcallosal cingulate cortex in patients with treatment resistant depression. *Psychiatry Research—Neuroimaging*, *261*, 72–74.

Van Essen, D. C., Smith, S. M., Barch, D. M., TEJ, B., Yacoub, E., Ugurbil, K., & Consortium W-MHCP. (2013). The WU-Minn human connectome project: An overview. *NeuroImage*, *80*, 62–79. https://www.ncbi.nlm.nih.gov/pubmed/23684880

Von Der Heide, R. J., Skipper, L. M., Klobusicky, E., & Olson, I. R. (2013). Dissecting the uncinate fasciculus: Disorders, controversies and a hypothesis. *Brain*, *136*, 1692–1707.

Wu, J., Buchsbaum, M. S., Gillin, J. C., Tang, C., Cadwell, S., Wiegand, M., … Bunney, W. E. (1999). Prediction of antidepressant effects of sleep deprivation by metabolic rates in the ventral anterior cingulate and medial prefrontal cortex. *The American Journal of Psychiatry*, *156*, 1149–1158.

SUPPORTING INFORMATION

Additional supporting information may be found online in the Supporting Information section at the end of this article.

How to cite this article: Tsolaki E, Sheth SA, Pouratian N. Variability of white matter anatomy in the subcallosal cingulate area. *Hum Brain Mapp*. 2021;42:2005–2017. https://doi.org/10.1002/hbm.25341